IEEE Photonics Journal
An IEEE Photonics Society Publication



# Mechanism of Improved Luminescence Intensity of Ultraviolet Light Emitting Diodes (UV-LEDs) Under Thermal and Chemical Treatments

Volume 11, Number 6, December 2019

Moheb Sheikhi
Wei Guo
Yijun Dai
Mei Cui
Jason Hoo
Shiping Guo
Liang Xu
Jianzhe Liu
Jichun Ye

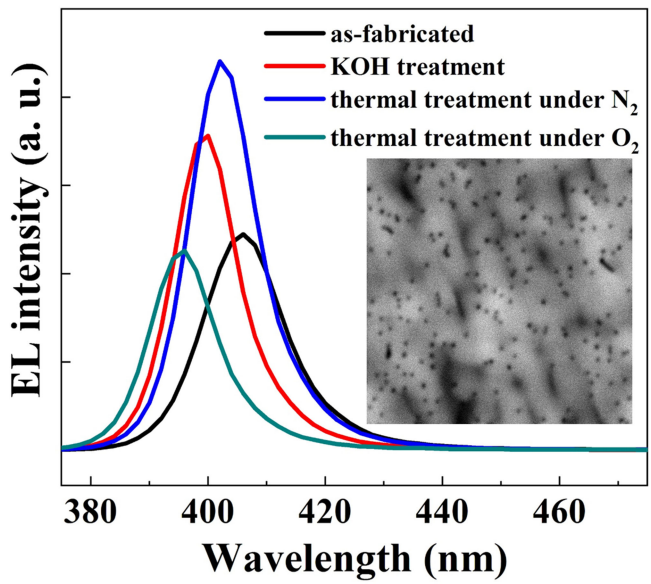


DOI: 10.1109/JPHOT.2019.2950049

IEEE photonics SOCIETY
IEEE

# Mechanism of Improved Luminescence Intensity of Ultraviolet Light Emitting Diodes (UV-LEDs) Under Thermal and Chemical Treatments

**Moheb Sheikhi,[1,2] Wei Guo ,[1,2] Yijun Dai,[1,2] Mei Cui,[1,2] Jason Hoo,[3] Shiping Guo,[3] Liang Xu,[4] Jianzhe Liu,[4] and Jichun Ye[1,2]**

[1]Ningbo Institute of Materials Technology and Engineering, Chinese Academy of Sciences, Ningbo 315201, China
[2]University of Chinese Academy of Sciences, Beijing 100049, China
[3]Advanced Micro-Fabrication Equipment, Inc., Shanghai 201201, China
[4]Zhejiang Bright Semiconductor Technology Company, Ltd., Jinhua 321000, China

*DOI:10.1109/JPHOT.2019.2950049*


Manuscript received September 26, 2019; revised October 22, 2019; accepted October 24, 2019. Date of publication October 28, 2019; date of current version December 16, 2019. This work was supported in part by the National Key Research and Development Program of China under Grant 2016YFB0400802; in part by the National Natural Science Foundation of China under Grants 61974149, 61704176, 61974178, and 61874177; in part by the Key Research and Development Program of Zhejiang Province under Grant 2019C01080; and in part by the Ningbo "Innovation 2025" Major Project under Grant 2018B10050. (Moheb Sheikhi and Wei Guo contributed equally to this work.) Corresponding authors: Wei Guo; Jichun Ye (e-mail: guowei@nimte.ac.cn; jichun.ye@nimte.ac.cn).

**Abstract:** In this work, the influences of thermal annealing and chemical passivation on the optical and electrical properties of ultraviolet light-emitting-diode (UV-LED) were investigated. The electroluminescence (EL) intensities of the LEDs under KOH treatment and thermal annealing increased by 48% and 81%, respectively compared to as-fabricated LED under current level of 10 mA. Cathodoluminescence (CL) mapping of UV-LEDs confirmed no variation of the density of the non-radiative recombination centers after surface treatments, and no obvious change in surface morphology was identified due to lacking of energy for surface atom migration. However, Raman spectroscopy indicates a relaxation of compressive strains inside the thin film after both thermal and chemical treatments, and conductive atomic force microscopy (c-AFM) also illustrated reduced leakage current after KOH passivation, which are responsible for the improved luminescence properties of UV-LEDs.

**Index Terms:** UV-LED, surface treatment, electroluminescence, strain relaxation.

## 1. Introduction

III-nitride wide bandgap semiconductors have attracted great interests among researchers due to their wide applications in light emitting diode (LED), laser diode (LD), and electronic electronics [1]–[3]. Due to strong spontaneous polarization in wurtzite crystals, polarization-induced charges and surface states influence the electrical and optical properties of III-nitride devices [4]. Additionally, high density of treading dislocations or point defects are also responsible for the increased non-radiative recombination rate and deterioration of device performance. Therefore, post-growth treatments have been widely utilized in III-nitride optoelectronic and electronic devices. In the fabrication of electronic devices, $SiO_2/SiN_x$ deposition or plasma treatment was usually applied in order to reduce surface traps and defects [5], which act as current leakage paths [3], [6]. For instance, it

was shown by Yang *et al*. that, reverse leakage current of Schottky-Barrier-Diode (SBD) was greatly reduced by oxygen plasma passivation, and the effective barrier height and ideality factor of the device were also improved [7]–[10]. In optoelectronic devices, similar passivation techniques can be found in literatures, especially in LDs operating under high current level [11], [12]. Thermal annealing was also performed after device fabrication, mainly post-metallization annealing for Ohmic contact optimization [13], [14], or p-GaN activation [15].

Nevertheless, little work has been done in investigating the influence of thermal or chemical treatments on the performances of LEDs, especially ultraviolet (UV) LEDs, which are critically important [16], [17]. This is because, firstly, dislocations and point defects are strongly correlated with internal quantum efficiency (IQE) of UV-LEDs as reported by Ban *et al.* [18], and thus must be reduced to a maximum extent; Secondly, surface defects and traps could lead to fermi level pinning and introduce barrier height between metal and GaN contact layer [19], [20]. Therefore, an easy and scalable post-growth treatment technique is strongly desired.

Recently, a few investigations on the chemical treatment of nanowire InGaN based UV-LEDs were carried out by researchers. For example, 50% enhancement in the UV light emission intensity was demonstrated from the KOH treated InGaN nanowires due to the removal of surface dangling bonds [17]. However, nanostructure-based LEDs suffer from large density of states at the free sidewalls and huge on-state resistance due to difficulties in current injection. This greatly holds back the development of high-efficiency UV-LEDs. Moreover, as the emission wavelength of UV-LED becomes shorter, external quantum efficiency (EQE) is severely degraded due to worse crystalline quality and less efficient carrier injection. Appropriate post-growth treatments on planar-structured UV-LEDs are expected to reduce non-radiative recombination centers, promote current injections and consequently, improve device performance [21]–[24].

In this work, we propose the use of diluted potassium hydroxide (KOH) solution and thermal treatment by rapid thermal annealing (RTA) to treat the as-fabricated UV-LEDs prior to metallization. Enhanced electroluminescence intensity was observed, which can be clearly demonstrated by a combination effect of strain relaxation and surface passivation.

## 2. Experiment

UV-LEDs were grown on 2-inch patterned sapphire substrates (PSS) via an AMEC Prismo HiT3$^{TM}$ metalorganic chemical vapor deposition (MOCVD). Trimethylaluminum (TMAl), triethylgallium (TEGa) and ammonia ($NH_3$) were used as precursors of Al, Ga and N, respectively. Hydrogen ($H_2$) was used as the carrier gas. The LED consists of 5 $\mu$m undoped GaN epitaxial layer, 1.5 $\mu$m Si-doped GaN contact layer, six pairs of unintentional doped $In_{0.07}Ga_{0.93}N$/GaN multiple quantum wells (MQWs), 14 nm Mg-doped GaN electron-blocking layer, and 500 nm Mg-doped p-GaN contact layer. The structure design is also illustrated in Fig. 1(a). Emission wavelength is targeted around 395 nm.

Circular-shape LED as shown in Fig. 1(b) was achieved by using a SUSS MA6 mask aligner to define the mesas, followed by reactive ion etching (RIE) of 600 nm depth towards the n-GaN contact layer via a Plasmalab System 100 ICP180 ICP-RIE system. Prior to metal contact deposition, various chemical and thermal treatments were applied to the LEDs. For chemical treatment, samples were dipped into KOH aqueous solution with a concentration of 10 wt%. KOH etching with temperature ranging from 25 °C to 60 °C for 30 s–300 s were performed. It is found that if the temperature is higher than 45 °C or the treatment time is longer than 40 s, the EL intensity of the UV-LED reaches saturation without further increasing. Therefore, the conditions of 45 °C and 40 s are utilized in this work. Regards to thermal treatment, RTA was performed at 800 °C for 15 min under $N_2$ or $O_2$ atmosphere, with ramping up speed of 20 °C/s and naturally ramping down to room temperature. Ring-shape Ohmic contact consisting Ti/Al/Ni/Au (10/120/30/30 nm) stack was then deposited on n-GaN contact layer via a Xingnan ZZS500 e-beam evaporation system. P-type contact consisting of Ni/Au (30/60 nm) stack was deposited in the center of the mesa.

Surface morphologies of the LEDs were characterized by Olympus optical microscopy and Veeco dimension 3100 V atomic force microscopy (AFM). For the conductive-AFM (cAFM) measurements,

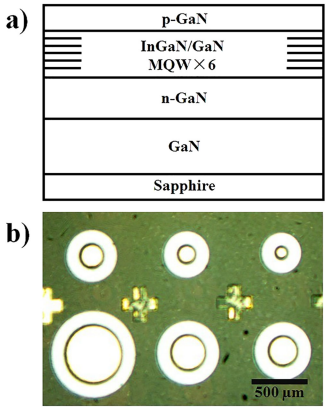


Fig. 1. Schematic structure of UV-LED (a). Top-view optical microscopy image of the sample with Ohmic contact deposited (b).

the microscope was operated under contact mode. The current mapping was recorded simultaneously with the topography. Electroluminescence (EL) spectra of the LEDs were characterized by a probe system, with luminescence collected by a Zolix Omni-λ300i spectrometer. Current–voltage (I–V) characteristic of the LEDs were analyzed by Keithley 4200-SCS semiconductor characterization system. Cathodoluminescence (CL) measurement was carried out to investigate the spatially-resolved luminescence properties using a 5 kV electron gun with a Gatan Mono CL4 system equipped with a Princeton PIXIS CCD with collection wavelength between 300 and 1100 nm. Finally, strain conditions of the LEDs were investigated by a Renishaw inVia Reflex spectrometer system with a 532 nm frequency-doubled Nd:YAG as the excitation source.

## 3. Results

Fig. 2(a) shows the EL spectra of the as-fabricated LEDs and after chemical and thermal treatments. Forward current was kept constant at 10 mA. As the size of the LED mesa is $2 \times 10^{-3}$ cm$^2$, EL characterization was performed at current density of 5 A/cm$^2$. Data collection were taken at several spots on the sample, and the EL spectra shown in the graph are averaging over the data in several spots. It is clearly observed that after KOH treatment and thermal treatment under $N_2$, EL intensity increased by ∼48% and 81% compared to that of the as-fabricated LED, suggesting that luminescence properties of the LEDs were dramatically improved. However, after thermal treatment under $O_2$ atmosphere, EL intensity decreased slightly by ∼7.5%. After thermal and chemical treatments, all spectra show blue shifts of approximately 10 nm compared to the as-fabricated LED. Both chemical and thermal treatments are not expected to influence the dislocation density due to lacking of energy for dislocation migration or thin film re-crystallization. Therefore, the observed blue shift could be explained by the change of bi-axial strains inside the LEDs or In localization [25]. Emission wavelengths are not the same after different treatments, which can be explained by the variation of strain states after post-fabrication treatment. Among all treatments, thermal annealing under $N_2$ shows the strongly EL intensity enhancement. This could be attributed to various reasons. Firstly, plasma-related damages induced by LED mesa etching can be readily healed by thermal annealing both at the sidewalls of MQWs and top surface of the n-contact layer, reducing the density of surface traps; Secondly, thermal annealing would promote Indium localization in the quantum well (QW) region, preventing carriers recombine non-radiatively in the dislocations or point defects; Last of all, thermal annealing would relax the bi-axial strains, reducing quantum-confined-stark-effect (QCSE) [26]–[28]. Regards to chemical treatment, it is anticipated that KOH etchants can passivate the surface by removal of either trap states or the polycrystalline nitride material introduced by plasma-related damages, thus increasing IQE [17]. Moreover, it it

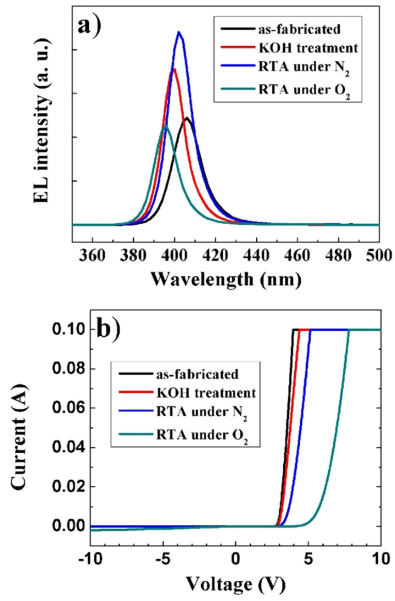


Fig. 2. EL spectra (a) and I-V curves (b) of the UV-LED samples subject to various post-growth treatments.

was reported that RIE of the surface of n-GaN contact layer creates extra electrons and lowers the barrier height between metal/semiconductor interface, which is critical in lowering the forward resistance [29]. Therefore, even though the past-fabrication techniques can passivate the surface defects, it may increases the series resistance of the LED devices, leading to less steep I-V curve.

In Fig. 2(b), I-V relationship of all UV-LEDs are compared. All I-V curves exhibit diode-like behavior, and the turn-on voltage for as-fabricated LED is ~2.92 V, slightly lower (7.5%) than the band-gap energy of InGaN quantum wells, which is 3.14 eV. This can be explained by the existence of current leakage paths inside LEDs. The I–V curves of the LEDs after chemical treatment show no significant difference compared to that of as-fabricated LED. However, after thermal annealing, the electrical properties of the LEDs were greatly changed. The turn-on voltages for LEDs after $N_2$ and $O_2$ annealing are ~3.43 V, and ~5.35 V, suggesting increases in turn-on voltages of 17.5% and 83% respectively. The turn-on voltage of LED after $O_2$ annealing is significantly increased, which might due to the formation of surface oxides, which increase the contact resistivity. The degradation of electrical property of LED under $O_2$ annealing is consistent with the decreased EL intensity as shown in Fig. 2(a). Additionally, reverse leakage current also increased for thermal annealing under $O_2$ atmosphere.

To understand the spatially-resolved luminescence properties of the LEDs under various post-growth treatments, room temperature CL characterization was performed on top of the LED mesa prior to p-electrode deposition. Under an acceleration voltage of 5 kV, the penetration depths of the electrons are a few $\mu$m, thus luminescence signals from the whole LED epi-structure can be collected. Monochromatic CL mappings at ~395 nm, which is the peak position of as-fabricated LED, are shown in Fig. 3. Dark spots featuring threading dislocations (TDs) and other defects in the thin film are visualized throughout the mapping, acting as non-radiative recombination centers. The dark-spot-density (DSD) is calculated to be $2.13 \times 10^8$ cm$^2$ for as-fabricated LEDs, no dramatic change in DSD is observed for thermal annealed LEDs under $N_2$ and KOH treated LEDs ($2.05 \times 10^8$ cm$^2$ and $2.19 \times 10^8$ cm$^2$ respectively). DSD slightly increased to $2.46 \times 10^8$ cm$^2$ for thermal annealed by $O_2$ atmosphere sample, also in accordance with the inferior EL performance as shown before. This result is further supported by the high-resolution XRD rocking curve (RC) scans of the LEDs,

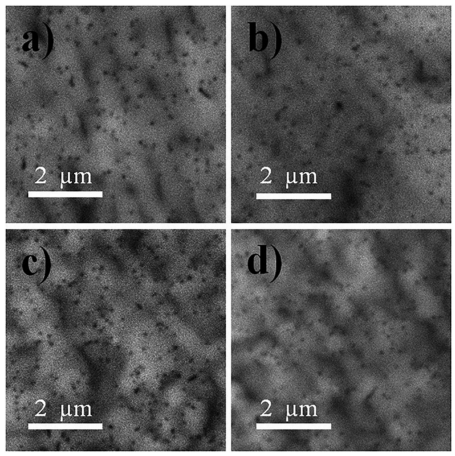


Fig. 3. Monochromatic CL intensity mappings of the as-fabricated LED (a), and LEDs after KOH treatment (b), thermal annealing under $N_2$ (c) and thermal annealing under $O_2$ (d).

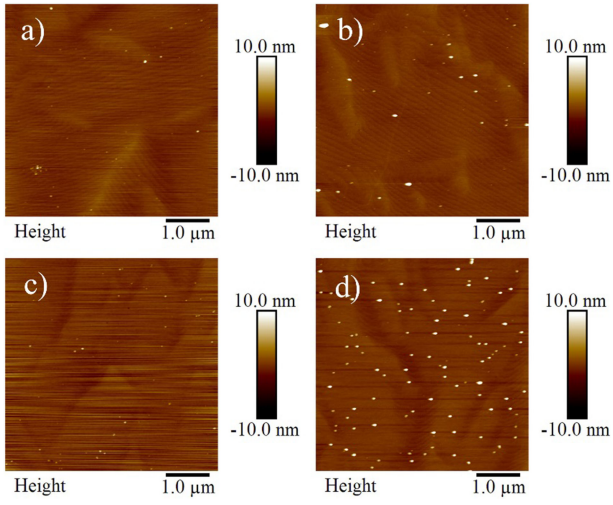


Fig. 4. AFM images of as-fabricated LED (a), and LED with KOH treatment (b), thermal annealing under $N_2$ atmosphere (c) and $O_2$ atmosphere (d).

and no obvious difference of the full-width-half-maximum values of the (002) and (102) RC scans is identified between as-fabricated LEDs and LEDs after post-growth treatments. It is speculated that threading dislocations are neither reduced nor passivated in the bulk, but the surface trap states which are related to the threading dislocations were possibly passivated, contributing to the enhanced EL intensities.

As shown in Fig. 2(b), the increased turn-on voltage for LEDs after $O_2$ thermal treatment is an indication of Ohmic contact degradation. This could possibly due to the formation of surface oxides and thus creation of Schottky barrier at the semiconductor/metal interface. To demonstrate this hypothesis, AFM surface morphologies on top of the LED mesa, i.e., p-type GaN of the LED with and without post-growth treatments are shown in Fig. 4. Clear bi-layer steps representing step-flow growth mode of p-GaN are observed on the as-fabricated and KOH treated LEDs. After thermal annealing, the bi-layer steps are less obvious, but the surface roughness remain similar. For KOH treated and thermal annealed LEDs under $O_2$ atmosphere, bumps of 100 nm diameter with a density of $3.76 \times 10^8$ $cm^2$ are uniformly distributed on the surface, attributing to the formation

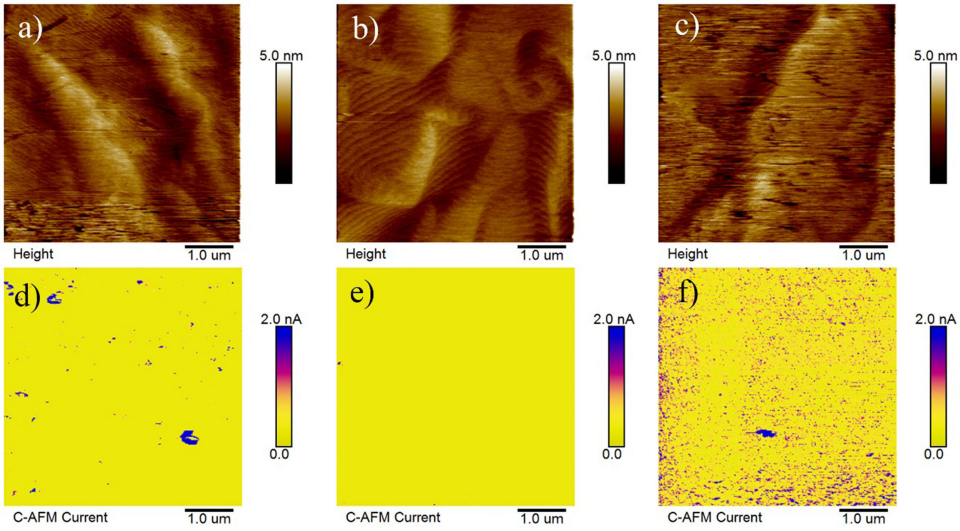


Fig. 5. Contact-mode AFM topographies of as-fabricated LED (a) and LED after KOH (b) and thermal annealing under $N_2$ (c) treatments, respectively; cAFM mapping showing the current leakage of corresponding LED samples at V = 3 V (d–f).

of gallium oxide or aluminum oxide particles. Surface roughness increased from 0.59 ± 0.02 nm for as-fabricated LED to 0.95 ± 0.02 nm for LED after thermal treatment by $O_2$. The existence of surface oxides and roughened surface lead to the inferior Ohmic contact property of the LED devices.

The current mappings performed by cAFM with corresponding topography images are further shown in Fig. 5, where the applied voltage is 3 V, and the current range is from 0 to 2 nA. The areas with blue or red dots are expected to be associated with the surface defects, which are responsible for the increased leakage current. In as-fabricated LED, a large defect spot with leakage current over 10 nA is clearly shown on the corner of the image, but no direct correlation between the surface morphology and current distribution is found. For LED after KOH treatment, no current leakage path is observed throughout the surface thanks to KOH passivation effect. Even though clear improvement is noticed for LED after chemical treatment, worse current distribution is shown for LED after $N_2$ annealing. Note that the density of the leakage paths is higher for LED after $N_2$ annealing than that of the as-fabricated sample, but the average current level is less than 1 nA. The exact mechanism responsible for this phenomenon is not clear at this moment. But we anticipate that it might be correlated to surface roughening and worse metal contact formation after thermal annealing. Considering that EL intensity is stronger for LED after thermal annealing under $N_2$ despite of existing current leakage paths, it is believed that other factors must be responsible for the improved device performance.

Last of all, bi-axial strain conditions were investigated by Raman spectroscopy. The room temperature Raman spectra of the LEDs with and without post-growth treatments are shown in Fig. 6(a). The peak position of the $E_2$ (high) phonon mode of III-nitride crystal is sensitive to bi-axial strains [30]. Compared to strain-free position, smaller Raman wavenumber suggests tensile strain, while larger Raman wavenumber suggests compressive strain. According to Tian *et al.* $E_2$ (high) position of a strain-free bulk GaN is located at 567.6 $cm^{-1}$ at 300 K. Thus the $E_2$ (high) position of ~572.1 $cm^{-1}$ for as-fabricated LED indicates a compressive strain of 1.76 GPa, if a stress coefficient of 2.56 $cm^{-1}$/GPa was utilized [31]–[33]. After KOH treatment and thermal treatment under $O_2$, $N_2$, the $E_2$ (high) positions shifted to lower values of ~569.6 $cm^{-1}$, ~569.6 $cm^{-1}$ and ~568.7 $cm^{-1}$, respectively, suggesting a relaxation of compressive strains. This could lead to decreased QCSE and consequently stronger radiative recombination rate inside the MQWs. Raman spectroscopy

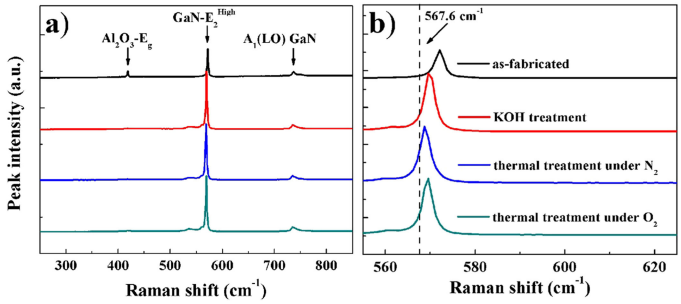


Fig. 6. Full-range (a) and zoom-in (b) Raman spectra of as-fabricated LED and after chemical and thermal treatments.

also agrees perfectly with the blue shifts of EL luminescence peaks shown in Fig. 2, since reduced QCSE usually lead to less severe band bending and higher bandgap energy.

## 4. Conclusion

In this article, we demonstrated improved EL intensity of the UV-LEDs after thermal and chemical treatments. CL mapping, cAFM and Raman spectroscopy were used to study the defect distribution, current leakage and strain conditions, respectively, shedding light into the physical mechanisms that directly influence the performance of UV-LED. LED after $N_2$ annealing exhibits the strongest EL intensity enhancement of 81% and reduced forward leakage current compared to as-fabricated LED, while dislocation or point defect densities in the bulk are not obviously changed as revealed by CL mapping. This study provides deeper understanding on the influence of post-growth treatments on the optical and electrical behaviors of the optoelectronic devices, and helps in further development of high-efficiency UV emitters.

## References

[1] B. Roul, M. Kumar, M. K. Rajpalke, T. N. Bhat, and S. B. Krupanidhi, "Binary group III-nitride based heterostructures: Band offsets and transport properties," *J. Phys. D, Appl. Phys.*, vol. 48, no. 42, 2015, Art. no. 423001.
[2] M. Kneissl, T.-Y. Seong, J. Han, and H. Amano, "The emergence and prospects of deep-ultraviolet light-emitting diode technologies," *Nature Photon.*, vol. 13, no. 4, pp. 233–244, 2019.
[3] M. Sheikhi *et al.*, "Polarity control of GaN and realization of GaN Schottky barrier diode based on lateral polarity structure," *IEEE Trans. Electron. Devices*, vol. 64, no. 11, pp. 4424–4429, Nov. 2017.
[4] M. Stutzmann *et al.*, "Playing with polarity," *Physica Status Solidi (B)*, vol. 228, no. 2, pp. 505–512, 2001.
[5] S. C. Binari *et al.*, "Trapping effects and microwave power performance in AlGaN/GaN HEMTs," *IEEE Trans. Electron. Devices*, vol. 48, no. 3, pp. 465–471, Mar. 2001.
[6] S. C. Binari, W. Kruppa, H. B. Dietrich, G. Kelner, A. E. Wickenden, and J. A. Freitas, "Fabrication and characterization of GaN FETs," *Solid-State Electron.*, vol. 41, no. 10, pp. 1549–1554, 1997.
[7] L. Yang, B. Zhang, Y. Li, and D. Chen, "Improved Schottky barrier characteristics for AlInN/GaN diodes by oxygen plasma treatment," *Mater. Sci. Semicond. Process.*, vol. 74, pp. 42–45, 2018.
[8] H. Chiu, C. Yang, C. Chen, and C. Wu, "Quality of the oxidation interface of AlGaN in enhancement-mode AlGaN/GaN high-electron mobility transistors," *IEEE Trans. Electron Devices*, vol. 59, no. 12, pp. 3334–3338, Dec. 2012.
[9] C. M. Jeon and J.-L. Lee, "Enhancement of Schottky barrier height on AlGaN/GaN heterostructure by oxidation annealing," *Appl. Phys. Lett.*, vol. 82, no. 24, pp. 4301–4303, 2003.
[10] U. K. Mishra, P. Parikh, and W. Yi-Feng, "AlGaN/GaN HEMTs-an overview of device operation and applications," *Proc. IEEE*, vol. 90, no. 6, pp. 1022–1031, Jun. 2002.
[11] C.-T. Hung, S.-C. Huang, and T.-C. Lu, "Effect of passivation layers on characteristics of AlGaInP ridge waveguide laser diodes," *Opt. Laser Technol.*, vol. 59, pp. 110–115, 2014.
[12] J. Xie *et al.*, "Lasing and longitudinal cavity modes in photo-pumped deep ultraviolet AlGaN heterostructures," *Appl. Phys. Lett.*, vol. 102, no. 17, 2013, Art. no. 171102.
[13] W. Guo *et al.*, "Comparative study on luminescence extraction strategies of LED by large-scale fabrication of nanopillar and nanohole structures," *J. Phys. D, Appl. Phys.*, vol. 51, 2018, Art. no. 24LT01.
[14] N. Miura *et al.*, "Thermal annealing effects on Ni/Au based Schottky contacts on n-GaN and AlGaN/GaN with insertion of high work function metal," *Solid State Electron.*, vol. 48, no. 5, pp. 689–695, 2015.

[15] N. Maeda, M. Jo, and H. Hirayama, "Improving the light-extraction efficiency of AlGaN DUV-LEDs by using a superlattice hole spreading layer and an Al reflector," *Physica Status Solidi A, Appl. Mater. Sci.*, vol. 215, no. 8, Apr. 2018, Art. no. 1700436.
[16] C.-H. Lin *et al.*, "Thermal annealing effects on the performance of a Ga-doped ZnO transparent-conductor layer in a light-emitting diode," *IEEE Trans. Electron Devices*, vol. 62, no. 11, pp. 3742–3749, Nov. 2015.
[17] H. Sun *et al.*, "Surface-passivated AlGaN nanowires for enhanced luminescence of ultraviolet light emitting diodes," *ACS Photon.*, vol. 5, no. 3, pp. 964–970, 2018.
[18] K. Ban *et al.*, "Internal quantum efficiency of whole-composition-range AlGaN multiquantum wells," *Appl. Phys. Exp.*, vol. 4, no. 5, 2011, Art. no. 052101.
[19] S. Keller *et al.*, "Optical and structural properties of GaN nanopillar and nanostripe arrays with embedded InGaN/GaN multi-quantum wells," *J. Appl. Phys.*, vol. 100, no. 5, 2006, Art. no. 054314.
[20] P. D. C. King, T. D. Veal, P. H. Jefferson, C. F. McConville, H. Lu, and W. J. Schaff, "Variation of band bending at the surface of Mg-doped InGaN: Evidence of p-type conductivity across the composition range," *Phys. Rev. B*, vol. 75, no. 11, 2007, Art. no. 115312.
[21] M. Hetzl *et al.*, "Surface passivation and self-regulated shell growth in selective area-grown GaN–(Al,Ga)N core–shell nanowires," *Nanoscale*, vol. 9, no. 21, pp. 7179–7188, 2017.
[22] J. I. Khan *et al.*, "Enhanced optoelectronic performance of a passivated nanowire-based device: Key information from real-space imaging using 4D electron microscopy," *Small*, vol. 12, no. 17, pp. 2313–2320, 2016.
[23] P. Varadhan *et al.*, "Surface passivation of GaN nanowires for enhanced photoelectrochemical water-splitting," *Nano Lett.*, vol. 17, no. 3, pp. 1520–1528, 2017.
[24] C. Zhao *et al.*, "An enhanced surface passivation effect in InGaN/GaN disk-in-nanowire light emitting diodes for mitigating Shockley–Read–Hall recombination," *Nanoscale*, vol. 7, no. 40, pp. 16658–16665, 2015.
[25] T. H. Seo, A. H. Park, G. H. Lee, M. J. Kim, and E.-K. Suh, "Efficiency enhancement of nanorod green light emitting diodes employing silver nanowire-decorated graphene electrode as current spreading layer," *J. Phys. D, Appl. Phys.*, vol. 47, no. 31, 2014, Art. no. 315102.
[26] W. Guo *et al.*, "Lateral-polarity structure of AlGaN quantum wells: A promising approach to enhancing the ultraviolet luminescence," *Adv. Functional Mater.*, vol. 28, 2018, Art. no. 1802395.
[27] Y.-Y. Chung *et al.*, "Quantum-well-width dependencies of postgrowth thermal annealing effects of InGaN/GaN quantum wells," *J. Appl. Phys.*, vol. 93, no. 12, pp. 9693–9696, 2003.
[28] H.-S. Chen *et al.*, "Strain relaxation and quantum confinement in InGaN/GaN nanoposts," *Nanotechnology*, vol. 17, no. 5, pp. 1454–1458, 2006.
[29] S. N. Mohammad, "Contact mechanisms and design principles for nonalloyed ohmic contacts to n-GaN," *J. Appl. Phys.*, vol. 95, no. 9, pp. 4856–4865, 2004.
[30] P. Perlin *et al.*, "Raman scattering and x-ray-absorption spectroscopy in gallium nitride under high pressure," *Phys. Rev. B*, vol. 45, no. 1, pp. 83–89, Jan. 1992.
[31] G. Sarau, M. Heilmann, M. Latzel, and S. Christiansen, "Disentangling the effects of nanoscale structural variations on the light emission wavelength of single nano-emitters: InGaN/GaN multiquantum well nano-LEDs for a case study," *Nanoscale*, vol. 6, no. 20, pp. 11953–11962, Oct. 2014.
[32] W. Tian *et al.*, "Tunability of intersubband transition wavelength in the atmospheric window in AlGaN/GaN multi-quantum wells grown on different AlGaN templates by metalorganic chemical vapor deposition," *J. Appl. Phys.*, vol. 112, no. 6, 2012, Art. no. 063526.
[33] D. Zhao, S. Xu, M. Xie, S. Tong, and H. Yang, "Stress and its effect on optical properties of GaN epilayers grown on Si (111), 6H-SiC (0001), and c-plane sapphire," *Appl. Phys. Lett.*, vol. 83, no. 4, pp. 677–679, 2003.